NJC

ROYAL SOCIETY OF CHEMISTRY

PAPER

Check for updates

Cite this: *New J. Chem.*, 2020, **44**, 14513

Received 14th April 2020,
Accepted 20th June 2020

DOI: 10.1039/d0nj01868f

rsc.li/njc

Influence of the adsorption of toxic agents on the optical and electronic properties of $B_{12}N_{12}$ fullerene in the presence and absence of an external electric field†

Alireza Soltani, *[a] Mohammad Ramezanitaghartapeh, [b] Masoud Bezi Javan,[c] Mohammad T. Baei,[d] Andrew Ng Kay Lup, [e] Peter J. Mahon[b] and Mehrdad Aghaei*[a]

The interaction energies and optoelectronic properties, in the presence and absence of an electric field, have been studied for the interaction of $B_{12}N_{12}$ with the toxic agents sarin (SF) and chlorosarin (SC) using density functional theory (DFT) and time-dependent density functional theory (TDDFT) calculations. The results demonstrate that the P═O group of SF and SC molecules can adsorb on the $B_{12}N_{12}$ with binding energies of −0.75 and −0.79 eV for the PBE functional, respectively. However, the binding energy of SC on $B_{12}N_{12}$ is slightly higher than that of SF. It was found that the electric field in the +*Y* direction increases the binding energies of the SF and SC molecules, while the electric field in the +*X* direction decreases the adsorption energy. Our computational results show the capability of $B_{12}N_{12}$ fullerene as a sensor for potential applications in the detection of toxic agents (SF and SC) under an external electric field.

1. Introduction

Significant attention has been paid towards the theoretical analysis, experimental synthesis and characterization of nanostructures composed of atoms other than carbon, especially those composed of Group 3 and 5 elements of the periodic table[1–5] owing to their electronic and optical properties that have offered excellent features for recent applications.[6–12] Recently, B_xN_x nano-cages, as isoelectronic fullerene analogues, have gained a great deal of attention from both synthetic and characterization points of view. Ring isomers (x = 3–10) and three-coordinated networks cages ($x > 10$) of B_xN_x have been recognized as the most stable configurations of this class of nanostructures.[13–16] To date, theoretical studies have been reported on the structural and electronic properties of B_xN_x clusters, where x equals 12, 20, 22, 24, 26, 28, 30, 32, 34 and 36.[17] These cages possess fascinating properties, such as oxidation resistance, low dielectric constant, high-temperature stability and large thermal conductivity.[18–21] There are two major classes of B_xN_x nano-cages, the first class includes the fullerene-like pentagonal and hexagonal structures with low structural strain and energetic disadvantages caused by N–N and B–B bonds. The alternative structures primarily contain energetically favorable B–N bonds through four- and six-membered rings that have sp^2 hybridization.[22–24] Taking this history of B_xN_x nano-cages into consideration, Oku *et al* revealed that $B_{12}N_{12}$ nano-cages are more stable than $B_{16}N_{16}$ and $B_{28}N_{28}$ nano-cages.[25]

It has been experimentally and computationally determined that external electric fields with controllable direction and intensity can be employed to modulate the interactions and electronic and optical properties of a nanostructure surface for a short time.[26] Many of these studies have been reported for carbon-based materials with various geometries.[27–32] Reports of experimental and theoretical implementations of external electric fields have demonstrated the electronic redistribution and enhanced adsorption capacity of nanostructures comprising carbon and boron–nitride nanostructures.[33] Owing to these exotic and fascinating properties, attention has recently been directed to the application of an external electric field in various studies, including adsorption processes.[34–36]

---

[a] *Golestan Rheumatology Research Center, Golestan University of Medical Science, Gorgan, Iran. E-mail: Alireza.soltani46@yahoo.com, alireza.soltani@goums.ac.ir, mehrdadaghaie@yahoo.com*

[b] *Department of Chemistry and Biotechnology, Swinburne University of Technology, Hawthorn, VIC 3122, Australia*

[c] *Physics Department, Faculty of Sciences, Golestan University, Gorgan, Iran*

[d] *Department of Chemistry, Azadshahr Branch, Islamic Azad University, Azadshahr, Golestan, Islamic Republic of Iran*

[e] *School of Energy and Chemical Engineering, Xiamen University Malaysia, Jalan Sunsuria, Bandar Sunsuria, 43900 Sepang, Selangor Darul Ehsan, Malaysia*

† Electronic supplementary information (ESI) available. See DOI: 10.1039/d0nj01868f

The nerve agent sarin (SF) can be produced from chlorosarin (SC) as a precursor and both chlorosarin and sarin are highly toxic with small doses being lethal upon adsorption.[37] Collombet and co-workers showed that the related nerve agent soman can affect blood and bone marrow micro-environments, thus preventing efficient bone marrow-derived stromal cell migration and engraftment.[38] Sarin has been shown to be an initiator of oxidative stress and, as a marker of oxidative degradation of DNA, 8-hydroxy-2′-deoxyguanosine was significantly elevated after intramuscular administration of the toxin into rats.[39] Therefore, their monitoring and adsorption are of great importance for environmental and health scientists.

Although there are numerous reports regarding the adsorption of sarin over amorphous SiO_2,[40] magnesium oxide,[41] a cement analogue surface,[42] monoclinic tungsten oxide,[43] graphane, graphene, and calcium oxide,[44] there are no reports in the literature on the interaction of sarin and chlorosarin molecules with $B_{12}N_{12}$ fullerene under an external electric field. Phenol adsorption on the surfaces of C_{24}, $B_{12}P_{12}$, $B_{12}N_{12}$, $Al_{12}N_{12}$, and $Al_{12}P_{12}$, with and without an electric field was studied using DFT calculations.[45] Baei *et al.* reported the use of BN nanotubes and $B_{12}N_{12}$ nano-cages as chemical sensors for N_2O gas with a parallel electric field.[46] Liu and Lee studied the effects of an electric field on the adsorption of CO on a graphene nanodot and their results demonstrated that an electric field can be applied to enhance CO adsorption.[47] Herein, to promote the interaction behavior of sarin and chlorosarin over $B_{12}N_{12}$ fullerene, two directional external electric fields were applied along the +*X* and +*Y* axes using DFT and TD-DFT calculations to determine the capability of $B_{12}N_{12}$ fullerene as a sensor and a promising adsorbent for the detection and removal of the toxic agents (SF and SC).

2. Computational details

Calculations of the adsorption behavior of sarin and chlorosarin over the surface of $B_{12}N_{12}$ fullerene, with and without an electric field (*F*), were performed initially. All the geometrical optimizations and energy calculations were obtained using the Gaussian 09 program package.[48] The level of density functional theory was based on the PBE,[49] B3LYP,[50] and M06-2X[51] functionals and the 6-311++G** standard basis set. The PBE and B3LYP density functionals have been previously applied in the study of BN nanostructures.[52–57] The spin multiplicity of the toxic molecules was set to one with relevance to its ground state molecular orbital (its ground electronic state is $^1\Sigma^+$). For all systems studied, the SCF convergence limit was set to 10^{-6} a.u. for energy and electron density calculations. For full optimization of the applied systems, SF and SC molecules are allowed to move freely across the surface of the $B_{12}N_{12}$ fullerene. The binding energy (E_b) of SF and SC molecules upon $B_{12}N_{12}$ fullerene is defined as follows:

$$E_b = E_{\text{Fullerene-nerve agent}} - (E_{\text{Fullerene}} - E_{\text{nerve agent}}) + E_{\text{BSSE}} \quad (1)$$

where $E_{\text{Fullerene-nerve agent}}$ is the total energy of the SF or SC molecule on the surface of the $B_{12}N_{12}$ fullerene. $E_{\text{Fullerene}}$ and $E_{\text{nerve agent}}$ are the total energies of the respective pure $B_{12}N_{12}$ fullerene and sarin/chlorosarin. The basis set superposition error (BSSE) for the adsorption energy was corrected by implementing the counterpoise method.

Natural bond orbital (NBO), Mulliken population analysis (MPA), and projected density of state (PDOS) analysis were carried out using the DFT/PBE functional and the 6-311++G** basis set. Using the previously relaxed structures, UV-visible electronic absorption spectra were calculated in the gas phase within the time-dependent density functional theory (TDDFT) methodology.[48] A total of 30 excited states for the fragments ($B_{12}N_{12}$ and toxic agents) and the corresponding complexes were calculated as vertical excitations. The influence of the static electric field on the structural, optical, and electronic properties of the $B_{12}N_{12}$ fullerene interacting with SF and SC molecules was investigated. All the studied systems were fully relaxed and all atoms in the adsorbate and adsorbent were allowed to move freely during the optimization process. The separate static external electric fields used in the +*X* and +*Y* directions are perpendicular to the +*X* and +*Y* planes. The numerical values of the static electric field strengths in the +*X* and +*Y* directions applied to the nerve agent–$B_{12}N_{12}$ systems are 0.005 and 0.010 a.u. (where 1 a.u. = 514.224 V nm^{-1}).[24] It has been observed that the influence of the static external electric field can be included by adding a field term in the Hamiltonian of the system, as reported by Wang and Farmanzadeh.[57,58]

3. Results and discussion

3.1. Geometric analysis

Fig. 1 shows the atomic labeling of SF and SC and the respective highest occupied molecular orbital (HOMO) and lowest unoccupied molecular orbital (LUMO) of the $B_{12}N_{12}$ fullerene, SF and SC molecules. The lengths of the $P{=}O_1$ and O_2–C_2 bonds increased with the adsorption on the $B_{12}N_{12}$ fullerene,[59] while the lengths of the P–O_2 and P–C_1 bonds decreased, as displayed in Table 1. At the same time, the bond distances and bond angles of the $B_{12}N_{12}$ fullerene increased, except in the case of the angle of N_1–B_1–N_2, which showed a decrease. SF and SC adsorb on $B_{12}N_{12}$ by chemisorption, as shown in the subsequent sections, which involves the partial transfer of charges or electron sharing from the oxygen atom of $P{=}O_1$ to the boron atom of the $B_{12}N_{12}$ fullerene. This sharing of electrons weakens the existing covalent bonding of the $P{=}O_1$ bond, causing it to increase in length. The change in the $P{=}O_1$ bond also affects the electron distribution within the adsorbate molecule itself, in which the electrons in the P–O_2 and P–C_1 bonds will be slightly shifted towards $P{=}O_1$, causing a change in the dipole moment of the adsorbate after adsorption. The redistribution of the electron cloud causes the lengths of the P–O_2 and P–C_1 bonds to decrease.

Fig. 2 shows a map of the electrostatic potential around the ethyl groups of SF and SC with the lone pairs of electrons on the nitrogen atoms of the $B_{12}N_{12}$ fullerene. In the figure, the points of positive and negative charge accumulation are separated

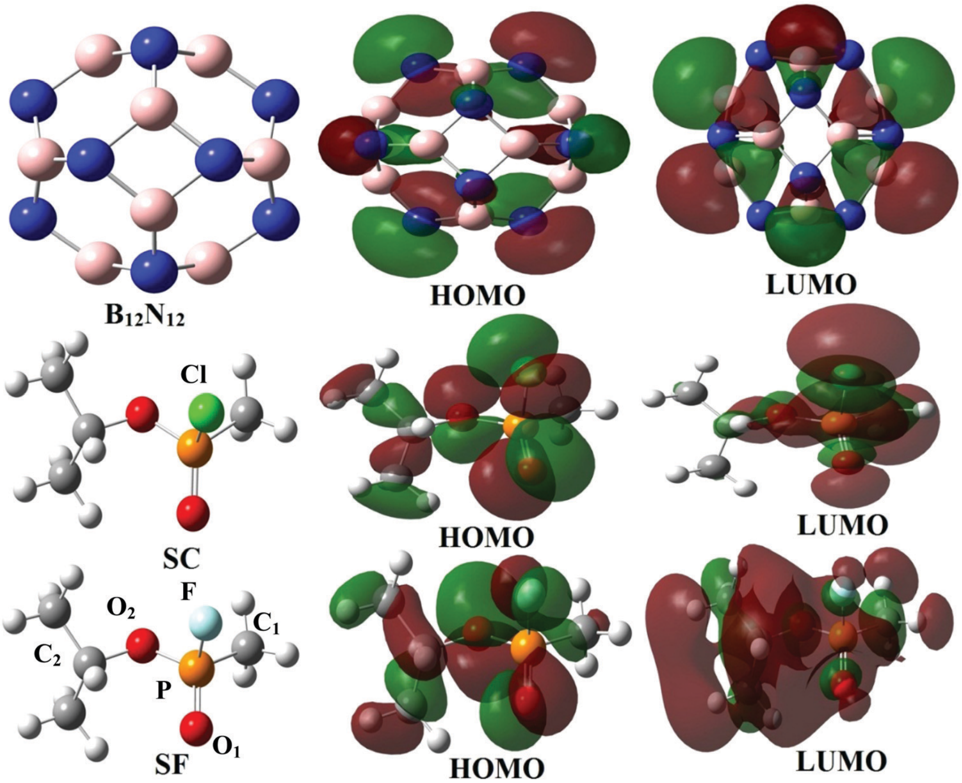

Fig. 1 Molecular structures, HOMO and LUMO of pure $B_{12}N_{12}$ fullerene, SC and SF molecules.

Table 1 Bond lengths, bond angles, E_{LUMO} and E_{HOMO}, dipole moments (μ_D/Debye), energy band gaps (E_g), Fermi level energy (E_F) and quantum molecular descriptors for SF and SC adsorption on $B_{12}N_{12}$ by PBE functional

Property	SF	SC	$B_{12}N_{12}$	SF–$B_{12}N_{12}$	SC–$B_{12}N_{12}$
$P{=}O_1$	1.489	1.493	—	1.523	1.537
$P–O_2$	1.616	1.620	—	1.579	1.589
$P–C_1$	1.803	1.808	—	1.788	1.794
$O_2–C_2$	1.483	1.482	—	1.517	1.510
$O_1{=}P–O_2$	117.46	117.67	—	118.25	116.38
$O_2–P–F$	111.14	—	—	109.76	—
$O_1{=}P–C_1$	—	111.16	—	—	104.64
$B–O_1{=}P$	—	—		134.70	128.97
$B_1–N_1$	—	—	1.493	1.583	1.576
$B_2–N_1$	—	—	1.445	1.484	1.475
$B_1–N_1–B_1$	—	—	80.15	83.11	84.15
$B_1–N_1–B_2$	—	—	110.57	116.27	116.68
$N_1–B_1–N_2$	—	—	98.48	92.05	91.52
E_{HOMO} (eV)	−7.0	−6.61	−7.03	−5.93	−6.01
E_{LUMO} (eV)	−0.79	−0.77	−2.04	−1.46	−2.27
E_g (eV)	6.21	5.84	4.99	4.47	3.74
ΔE_g (%)	—	—	—	10.42	25.05
E_F (eV)	−7.79	−7.38	−4.54	−3.70	−4.14
μ_D (Debye)	3.07	3.12	0.0	10.71	9.18
E_b (eV)	—	—	—	−0.75	−0.79
Q (e)	—	—	—	0.51	0.18
D (Å)	—	—	—	1.596	1.589
I (eV)	7.0	6.61	7.03	5.93	6.01
A (eV)	0.79	0.77	2.04	1.46	2.27
η (eV)	3.11	2.92	2.50	2.24	1.87
μ (eV)	−3.90	−3.69	−4.53	−3.70	−4.14
S (eV^{-1})	0.16	0.17	0.20	0.22	0.27
ω (eV)	2.44	2.33	4.12	3.05	4.58

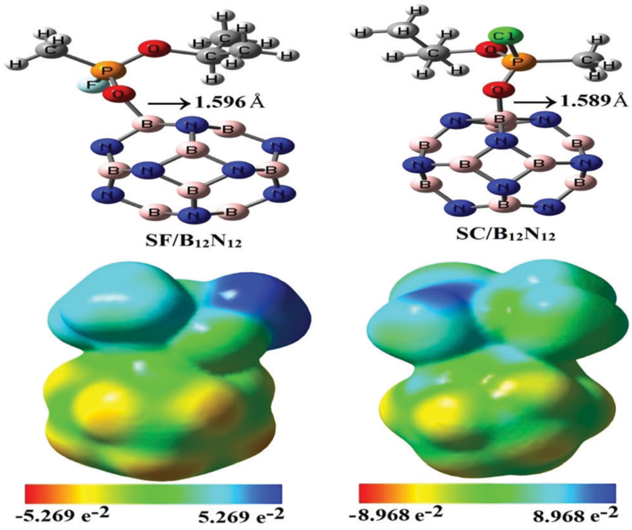

Fig. 2 The optimized geometries and their MEP plots for SF and SC molecules adsorbed over pure $B_{12}N_{12}$ fullerene.

from each other by blue and red colors, which indicates the enhancement of the coulombic repulsion effect at the surface of the $B_{12}N_{12}$ nanocage, causing the ethyl group to be slightly shifted away from the adsorbates ($O_2–C_2$ bond length increased) to mitigate these effects. The interaction of boron with oxygen involves the formation of a partial covalent bond with a boron atom, which transforms its default sp^2-hybridization with three other nitrogen atoms in the fullerene into an arrangement akin to sp^3-hybridization with longer bond lengths. In $B_{12}N_{12}$ fullerene, the boron exists on a quasi-square plane (B_1–N_1–B_1 and B_1–N_1–B_2) and two quasi-hexagonal planes (N_1–B_1–N_2), in which both bond angles will respectively increase and decrease to approach the bond angles of a quasi-sp^3-hybridization shape.[60]

However, the application of the external electric field has a significant effect on the geometric parameters of both the toxic agents and the $B_{12}N_{12}$ fullerene.[45,46] The field caused a further increase in the length of the P=O_1 bond, with the highest increase observed upon the application of E_Y = 0.01 a.u. to the SC/SF–$B_{12}N_{12}$ fullerene systems. The application of the external electric field further strengthened the electron redistribution effect of the adsorbate towards the P=O···B bond region. The perpendicular electric field (E_Y) had a greater effect than the parallel electric field (E_X) as the P=O_1 bond is aligned in the E_Y field during adsorption. This strengthened effect resulted in a further increase in the P=O_1 bond length and a decrease in the P–O_2 bond length. In the case of the P–C_1 bond, it was almost unchanged after the application of the external electric field to the SF and SC before the interaction with the $B_{12}N_{12}$ fullerene, while it negligibly decreased for almost all of the applied external electric fields except for E_X = 0.01 a.u. for the SF–$B_{12}N_{12}$ fullerene system.

The C_2–O_2 bond length first showed a decreasing trend with the application of the external electric field but then it increased after the interaction with the $B_{12}N_{12}$ fullerene and a similar trend was observed for the O_1=P–O_2 bond angle. The aforementioned electron redistribution effect caused by an external electric field resulted in the slight polarization of the C_2–O_2 electron cloud towards the P=O···B bond region but the effect was reversed upon adsorption owing to the steric and repulsion effects on the ethyl group by $B_{12}N_{12}$ fullerene. In a similar vein to this, the O_1=P–O_2 bond angle, which is dependent on electron repulsion, changed accordingly with the C_2–O_2 bond length change. The O_1=P–C_1 and B–O_1=P bond angles significantly changed before and after the application of the external electric field but when it comes to interaction with the $B_{12}N_{12}$ fullerene, the application of the external electric field does not make a big difference.

The initial bond lengths for B_1–N_1 and B_2–N_1 are 1.493 and 1.445 Å, respectively, but they increased slightly after the application of the external electric fields, except for the B_2–N_1 bond under external electric fields of E_X = 0.005 and 0.01 a.u. Such results are entirely compatible with those reported by Okada and Oshiyama[61] and Freitas *et al.*,[62] which demonstrated that the effect of an electric field on the structural properties of a MWBNNT is negligible. The lengths of the B_1–N_1 and B_2–N_1 bonds in the pure $B_{12}N_{12}$ fullerene were found to be 1.482 and 1.437 Å, respectively, by the M06-2X functional. Our calculations using the PBE functional are in good agreement with the theoretical results reported by Strout.[15] Additionally, the interactions of SF and SC with the $B_{12}N_{12}$ fullerene under an external electric field caused larger changes in the mentioned bond lengths. Regarding the angles of the B_1–N_1–B_1, B_1–N_1–B_2 and N_1–B_1–N_2 bonds in bare $B_{12}N_{12}$ fullerene, these results show that the application on an external electric field does not cause noticeable changes in the values of these angles while upon interaction with SF or SC significant changes were observed either with or without the application of an external electric field. These results show that a higher field strength causes greater changes in the bond lengths and bond angles. As depicted in Fig. 1, for the HOMO of $B_{12}N_{12}$ the charge density is located on 2p orbital of N atom, while in the LUMO the charge density is located on the 2p orbital of B atom. The HOMO and LUMO plots of SC and SF molecules are situated on the phosphoryl chloride and the carbon and oxygen atoms.

3.2. Adsorption on $B_{12}N_{12}$ fullerene

For adsorption of SF and SC on the $B_{12}N_{12}$ fullerene, various possible initial adsorption geometries were considered. After full structural optimization, the stable structures are shown and calculated. The interaction of SF and SC with the Lewis acid site of boron atoms of $B_{12}N_{12}$ fullerene in the gas phase has been studied using density functional theory calculations (Fig. 2). Theoretical reports regarding the adsorption of gas molecules[57,63–65] and amino acids[66–68] over the surface of $B_{12}N_{12}$ demonstrate that the interactions of adsorbates over the nitrogen atom of $B_{12}N_{12}$ fullerene typically involve physisorption due to weak van der Waals interactions, while these adsorbates typically interact with the boron atom of $B_{12}N_{12}$ fullerene by chemisorption. In $B_{12}N_{12}$ fullerene, the valence shell of nitrogen was completely bonded with three N–B bonds while boron still has a vacant orbital for adsorption after forming three N–B bonds. Fig. 2 and Table 1 show the relaxed models of SF and SC adsorbed by $B_{12}N_{12}$ fullerene through the sharing of electrons and connected by covalent bonds. For both interaction models, using the PBE functional, the binding energy values were calculated to be −0.75 and −0.79 eV, the B···O=P interaction distances were 1.596 and 1.589 Å, and the B···O=P bond angles were 134.70° and 128.97° for SF and SC, respectively. Both interaction models resulted in similar ranges as their respective availabilities of lone pair electrons in oxygen and dipole moments (μ_D = 3.07 and 3.12 Debye) are similar.

For comparison, the E_b values of SF and SC on $B_{12}N_{12}$ fullerene were computed using the M06-2X functional and the 6-311++G** basis set. The calculations indicated that there is a large difference in the binding energies obtained from the M06-2X and the PBE functionals as the E_b values for SF and SC adsorbed upon $B_{12}N_{12}$ fullerene were −1.12 and −1.17 eV, respectively (about 0.30–0.45 eV, depending on the agent). Fig. 3 shows the adsorption of SF and SC from their fluorine and chlorine heads upon $B_{12}N_{12}$ fullerene with respective binding energies of +0.32 (state Z) and +0.34 eV (state S) provided by the PBE functional. Both positive binding energies indicate that adsorption *via* halogen atoms is unfavorable. Thus, the adsorptions of SF and SC on $B_{12}N_{12}$ are dependent on the orientation of the adsorbates. Bermudez *et al.*[68] reported that the adsorption of sarin on the surface of Al_8O_{12} has a binding energy of −0.95 eV. Michalkova *et al.* reported on the

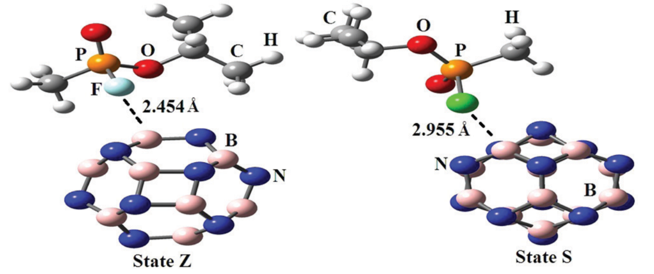

Fig. 3 Adsorption models for SF and SC molecules adsorbed by their fluorine and chlorine heads over pure $B_{12}N_{12}$ fullerene.

strong interactions between sarin (from its P═O head) and a MgO surface, finding an adsorption energy of −2.17 eV using the MP2 method.[41]

Based on MPA, charges of about 0.51 and 0.18 $|e|$ are transferred from SF and SC, respectively, as electron donors to $B_{12}N_{12}$ fullerene during interaction processes where $B_{12}N_{12}$ acts as an electron acceptor. The positive charge distributions on the SF and SC with blue color in the molecular electrostatic potential (MEP) plots indicate that the toxic agents function as electron donors and the fullerene with red-yellow color functions as an electron acceptor, as displayed in Fig. 2. The lengthened B_1–N_1 bond (1.493 Å in the free model to 1.583 Å (SF) and 1.576 Å (SC) in the interaction models) shows that the sp^2 hybridization of free $B_{12}N_{12}$ fullerene has altered to become sp^3 hybridization. The lengthened B_1–N_1 bond causes the boron atom to be displaced slightly outwards from the fullerene during adsorption, introducing a structural deformation on $B_{12}N_{12}$ fullerene. This deformation would cause a break in the centrosymmetry of the $B_{12}N_{12}$ structure in the *ZX* plane, which is a required condition for its zero dipole moment. The slight break in the centrosymmetry of the $B_{12}N_{12}$ structure results in a significant increase in the overall dipole moment of the adsorbate–adsorbent ensemble as the effect is accentuated by the large structure of the $B_{12}N_{12}$ fullerene.

3.3. Influence of the electric field

Calculations focusing on the effects of the external electric fields applied through the positive *X* (parallel to *ZX* plane), E_X and *Y* (perpendicular to *ZX* plane), E_Y directions on the interaction of SF and SC molecules with $B_{12}N_{12}$ fullerene using the PBE functional were compared with those using the B3LYP functional. The interaction energies and structural properties, with and without the presence of an electric field, were studied for the interaction of $B_{12}N_{12}$ with the toxic agents and the results are compared. Tables 2 and 3 show the energy shift for the $B_{12}N_{12}$ fullerene interacting with SF and SC molecules under an applied electric field *versus* the induced dipole moment. When the field was applied in the +*X* and +*Y* directions, which are parallel and perpendicular to the P═O bond, almost all the bond lengths and bond angles were changed accordingly.

These changes were attributed to the electron redistribution effect induced by the external electric field, as mentioned in Section 3.1. Such an effect on the topological properties at the bonds of interest can also be explained based on the polarizability of the bonding orbital of the donor molecule (toxic agents) with respect to that of the acceptor molecule ($B_{12}N_{12}$). When an electric field points from the donor to the acceptor,

Table 2 Bond lengths, bond angles, E_{LUMO} and E_{HOMO}, dipole moments (μ_D/Debye), energy band gaps (E_g), Fermi level energies (E_F) and quantum molecular descriptor values for pure SF, SC and $B_{12}N_{12}$ by PBE functional in the presence of an external electric field

	SF				SC				$B_{12}N_{12}$			
	E_X (a.u.)		E_Y (a.u.)		E_X (a.u.)		E_Y (a.u.)		E_X (a.u.)		E_Y (a.u.)	
Property	0.005	0.01	0.005	0.01	0.005	0.01	0.005	0.01	0.005	0.01	0.005	0.01
P═O_1	1.490	1.492	1.493	1.490	1.493	1.493	1.494	1.495	—	—	—	—
P–O_2	1.602	1.587	1.613	1.611	1.636	1.654	1.618	1.613	—	—	—	—
P–C_1	1.808	1.814	1.802	1.804	1.804	1.801	1.806	1.803	—	—	—	—
O_2–C_2	1.495	1.514	1.479	1.487	1.469	1.458	1.480	1.480	—	—	—	—
O_1═P–O_2	119.08	121.17	118.65	112.38	115.77	114.00	117.05	117.46	—	—	—	—
O_1–P–Cl	—	—	—	—	111.81	112.37	110.67	109.38	—	—	—	—
O_1–P–F	111.03	110.24	110.95	111.58	—	—	—	—	—	—	—	—
O_1═P–C_1	117.52	116.21	117.57	101.71	118.50	119.13	118.67	119.38	—	—	—	—
B_1–N_1	—	—	—	—	—	—	—	—	1.496	1.500	1.497	1.500
B_2–N_1	—	—	—	—	—	—	—	—	1.442	1.440	1.451	1.456
B_1–N_1–B_1	—	—	—	—	—	—	—	—	80.23	80.33	79.99	79.86
B_1–N_1–B_2	—	—	—	—	—	—	—	—	110.69	110.89	110.06	109.54
N_1–B_1–N_2	—	—	—	—	—	—	—	—	98.10	97.71	98.36	98.18
E_{HOMO} (eV)	−7.15	−7.20	−7.08	−7.54	−6.84	−6.77	−7.16	−7.30	−7.47	−7.86	−7.23	−7.39
E_{LUMO} (eV)	−1.23	−2.07	−0.84	−1.31	−1.38	−2.37	−1.40	−1.66	−2.53	−3.10	−2.29	−2.70
E_g (eV)	5.92	5.13	6.24	6.23	5.46	4.40	5.76	5.64	4.94	4.76	4.94	4.69
μ_D (Debye)	4.18	5.72	4.43	7.55	2.77	3.56	4.38	5.85	2.54	5.11	2.55	5.10
E_F (eV)	−4.19	−4.64	−3.96	−4.43	−4.11	−4.57	−4.28	−4.48	−5.0	−5.48	−4.76	−5.04
I (eV)	7.15	7.20	7.08	7.54	6.84	6.77	7.16	7.30	7.47	7.86	7.23	7.39
A (eV)	1.23	2.07	0.84	1.31	1.38	2.37	1.40	1.66	2.53	3.10	2.29	2.70
η (eV)	2.96	2.57	3.12	3.12	2.73	2.20	2.88	2.82	2.47	2.38	2.47	2.35
μ (eV)	−4.19	−4.64	−3.96	−4.43	−4.11	−4.57	−4.28	−4.48	−5.0	−5.48	−4.76	−5.04
S (eV^{-1})	0.17	0.19	0.16	0.16	0.18	0.23	0.17	0.18	0.20	0.21	0.20	0.21
ω (eV)	2.98	4.09	2.51	3.14	3.04	4.80	3.11	3.61	5.06	6.31	4.59	5.43

Table 3 Bond lengths, bond angles, E_{LUMO} and E_{HOMO}, dipole moments (μ_D/Debye), energy band gaps (E_g), change in band gaps (ΔE_g), Fermi level energies (E_F) and quantum molecular descriptor values for SF and SC adsorption on $B_{12}N_{12}$ by PBE functional in the presence of an external electric field

	SF–$B_{12}N_{12}$				SC–$B_{12}N_{12}$			
	E_X (a.u.)		E_Y (a.u.)		E_X (a.u.)		E_Y (a.u.)	
Property	0.005	0.01	0.005	0.01	0.005	0.01	0.005	0.01
$P{=}O_1$	1.519	1.516	1.531	1.540	1.533	1.526	1.547	1.558
$P{-}O_2$	1.576	1.572	1.566	1.553	1.585	1.582	1.579	1.564
$P{-}C_1$	1.796	1.806	1.787	1.788	1.795	1.796	1.794	1.792
$O_2{-}C_2$	1.528	1.539	1.528	1.543	1.516	1.521	1.518	1.527
$O_1{=}P{-}O_2$	120.50	122.95	119.40	117.36	117.51	118.66	116.57	111.32
$O_2{-}P{-}F$	110.44	110.96	108.14	107.77	—	—	—	—
$O_1{=}P{-}C_1$	—	—	—	—	104.42	104.42	103.77	107.89
$B_1{-}N_1$	1.573	1.544	1.585	1.575	1.576	1.551	1.582	1.591
$B_2{-}N_1$	1.490	1.478	1.482	1.471	1.481	1.488	1.473	1.464
$B_1{-}N_1{-}B_1$	82.80	83.72	83.53	84.48	83.46	83.59	84.44	84.93
$B_1{-}N_1{-}B_2$	115.80	116.04	117.12	118.73	115.89	115.64	117.20	118.80
$N_1{-}B_1{-}N_2$	92.84	93.66	91.58	91.27	92.30	93.38	91.07	90.09
E_{HOMO} (eV)	−6.59	−7.23	−5.94	−5.85	−6.70	−7.38	−6.02	−5.97
E_{LUMO} (eV)	−3.06	−5.02	−1.23	−2.03	−3.54	−4.87	−1.68	−2.09
E_g (eV)	3.53	2.21	4.71	3.82	3.16	2.51	4.34	3.88
ΔE_g (%)	28.54	53.57	4.66	18.55	36.03	47.27	12.14	17.27
E_F (eV)	−4.83	−6.13	−3.59	−3.94	−5.12	−6.13	−3.85	−4.03
μ_D (Debye)	7.95	7.46	15.06	21.14	7.26	8.49	14.40	22.07
E_b (eV)	−0.32	+0.08	−1.11	−1.41	−0.68	−0.60	−1.16	−1.76
D (Å)	1.636	1.689	1.561	1.536	1.634	1.712	1.551	1.518
I (eV)	6.59	7.23	5.94	5.85	6.70	7.38	6.02	5.97
A (eV)	3.06	5.02	1.23	2.03	3.54	4.87	1.68	2.09
η (eV)	1.77	1.11	2.36	1.91	1.58	1.26	2.17	1.94
μ (eV)	−4.83	−6.13	−3.59	−3.94	−5.12	−6.13	−3.85	−4.03
S (eV^{-1})	0.28	0.45	0.21	0.26	0.32	0.40	0.23	0.26
ω (eV)	6.59	16.97	2.73	4.06	8.29	14.95	3.42	4.19

i.e. $-Y$ field, the field polarizes the bonding orbital of the $P{=}O_1$ in the toxic agents away from the bonding region which is the empty orbital on the boron atom of $B_{12}N_{12}$. On the other hand, an electric field that points from the acceptor to the donor, *i.e.* $+Y$ field, will push the bonding orbital electrons towards the empty orbital.

Our calculations revealed that an increase in the electric field intensity leads to significant changes in the structural properties of both the adsorbent and the adsorbate. The value of E_b for SF adsorbed on the surface of $B_{12}N_{12}$ fullerene under an external parallel electric field (E_X = 0.005 a.u.) is −0.32 eV with a distance of 1.636 Å while the same interaction configuration under E_X = 0.010 a.u. revealed a binding energy of about +0.08 eV with a distance of 1.689 Å, demonstrating that the value of E_b decreased by about 0.4 eV owing to the higher electric field (Fig. S1, ESI† and Fig. 4). Under an external perpendicular electric field, the values of E_b increase for SF and SC chemisorbed on the surface of $B_{12}N_{12}$ fullerene.

In the same vein, the effects of an external electric field on the topological properties of the bonds subsequently affect the equilibrated distance and interaction energy between the adsorbate and adsorbent. At a long distance, the adsorbate–adsorbent complex becomes more stabilized as the adsorbate and adsorbent come closer together owing to the increase in mutual polarization, which strengthens their interaction. At shorter distances, covalent bonds at the terminal atoms of both molecules weaken and this destabilization effect controls the overall energy of the complex. By introducing an external electric field from the donor to the acceptor ($-Y$ field), the polarizing effect of the bonding orbital ($P{=}O_1$) away from the empty orbital of boron further enhances the destabilization effect on the complex and lengthens the equilibrium binding distance. On the other hand, a $+Y$ field will minimize the destabilization effect by increasing mutual polarization, thus stabilizing the adsorption complex and shortening the equilibrium binding distance.

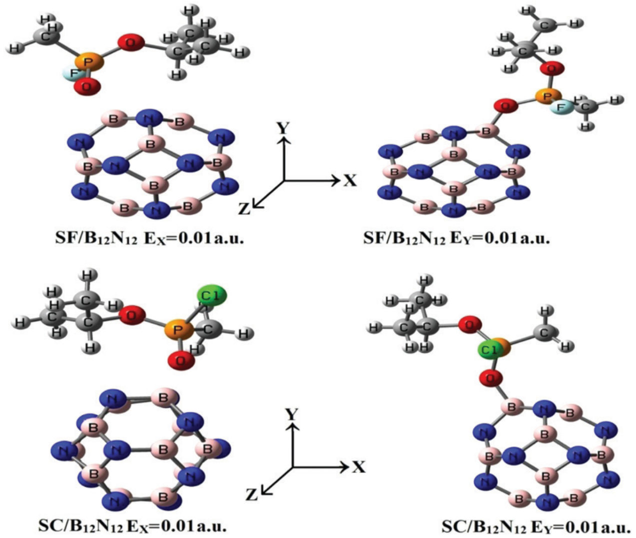

Fig. 4 Adsorption models for SF and SC molecules over $B_{12}N_{12}$ fullerene under electric field strengths of E_X = 0.01 a.u. and E_Y = 0.01 a.u.

Such weak interactions under an external parallel electric field reveal that desorption of the toxic agent could be easy and the device could suffer from short recovery times.[69,70] Conversely, the strong interactions are not important in toxic agent detection because these reveal that desorption from the fullerene could be difficult and the device may benefit from long recovery times. These results also indicate the possibility of real-time variation of the electric field strength and direction to manipulate the adsorption duration and amount for these toxic agents in this system.

MPA demonstrates that charges of about 0.486 and 0.419 $|e|$ are transferred from the SF to the fullerene under parallel electric field strengths of 0.005 and 0.010 a.u., respectively. In contrast, the binding energy between SF and $B_{12}N_{12}$ for E_Y = 0.005 and 0.010 a.u. are much more favored than those for E_X = 0.005 and 0.010 a.u., where the E_b values are −1.11 and −1.41 eV, respectively, and the distances between SF and $B_{12}N_{12}$ in E_Y = 0.005 and 0.010 a.u. are about 1.561 and 1.536 Å, respectively (Table 3), which is in agreement with previous DFT calculations.[71] Farmanzadeh and Ghazanfary indicated that glutamic acid and the amino acids lysine, glycine, and serine are considerably chemisorbed on BNNTs in the presence of an external electric field.[58] The charge-transfer mechanism, which is sometimes considered as an alternative to the electric field enhancement effect, is really significant as the interactions involve chemisorption and the charge transfer between the fullerene and the SF is considerable at electric field strengths of E_Y = 0.005 (0.522 $|e|$) and 0.010 a.u. (0.592 $|e|$).

In general, a lower E_b indicates higher sensitivity and a smaller response time for sensing applications, which is different from the results obtained by Kuila and coworkers.[72] The value of E_b considerably decreased in the parallel electric field (E_X = 0.01 a.u.), indicating that the electric field can enhance the sensing power of $B_{12}N_{12}$ fullerene for SF and SC detection. In contrast with the parallel electric field, perpendicular fields caused less of a decrease in the E_g, which was revealed by the previous theoretical study, showing that the coupling effect of the electric field and the radial deformation weaken the diminution of E_g.[73,74]

The effect of the computational methods on the adsorption of SF and SC on $B_{12}N_{12}$ was studied using the B3LYP functional in the presence of an external electric field (Table 4). Reports have shown that the two applied methods do not cause notable changes in the adsorption and physical properties of single molecules for structures like CNTs or graphene.[73,74] Herein, the computations showed that in the presence of E_X = 0.010 a.u., the length of the P=O$_1$ bond in SF is 1.516 Å (with the PBE functional) and 1.496 Å (with the B3LYP functional) after the interaction processes. The E_g of the structure from both methods was 2.21 eV for the interaction processes for the electric field of E_X = 0.010 a.u.

3.4. Nonlinear optical (NLO) properties

The broadening of the redshift of an adsorption peak in the presence of an external electric field is a common behavior in semiconductors[75] and is known as the Stark effect. Therefore, the behavior of Stark shifts with $B_{12}N_{12}$ is an important case study. In the presence of a permanent dipole moment (μ_0/Debye), the energy shift of a single molecule of $B_{12}N_{12}$ is linearly dependent on the applied electric field, while a quadratic dependence can be observed owing to the quantum-confined Stark

Table 4 Bond lengths, bond angles, E_{LUMO} and E_{HOMO}, dipole moments (μ_D/Debye), energy band gaps (E_g), change in band gaps (ΔE_g), Fermi level energies (E_F) and quantum molecular descriptor values of SF and SC adsorption on $B_{12}N_{12}$ by B3LYP functional in the presence of an external electric field

	$B_{12}N_{12}$		SF–$B_{12}N_{12}$		SC–$B_{12}N_{12}$	
Property	E_X = 0.01 a.u.	E_Y = 0.01 a.u.	E_X = 0.01 a.u.	E_Y = 0.01 a.u.	E_X = 0.01 a.u.	E_Y = 0.01 a.u.
P=O$_1$	—	—	1.496	1.519	1.508	1.542
P–O$_2$	—	—	1.556	1.530	1.566	1.550
P–C$_1$	—	—	1.800	1.788	1.792	1.788
O$_2$–C$_2$	—	—	1.533	1.559	1.515	1.521
O$_1$=P–O$_2$	—	—	121.80	115.00	117.66	111.67
O$_2$–P–F	—	—	110.63	107.41	—	—
O$_1$=P–C$_1$	—	—	—	—	105.20	107.35
B$_1$–N$_1$	1.493	1.501	1.537	1.578	1.554	1.598
B$_2$–N$_1$	1.432	1.456	1.473	1.465	1.435	1.469
B$_1$–N$_1$–B$_1$	80.85	79.87	82.80	84.71	83.55	84.40
B$_1$–N$_1$–B$_2$	111.47	109.53	116.25	119.20	115.68	119.96
N$_1$–B$_1$–N$_2$	97.32	98.17	93.45	90.67	92.97	89.79
E_{HOMO} (eV)	−8.80	−7.39	−7.23	−6.87	−8.25	−6.95
E_{LUMO} (eV)	−2.76	−2.70	−5.02	−1.96	−4.19	−1.96
E_g (eV)	6.04	4.69	2.21	4.91	4.06	4.99
ΔE_g (%)	—	—	63.41	4.69	32.78	6.40
E_F (eV)	−5.78	−5.04	−6.13	−4.42	−6.22	−4.46
μ_D (Debye)	5.0	5.11	7.51	14.89	8.62	21.74
E_b (eV)	—	—	−0.11	−1.55	−0.78	−1.90
D (Å)	—	—	1.704	1.519	1.703	1.513
I (eV)	8.80	7.39	7.23	6.87	8.25	6.95
A (eV)	2.76	2.70	5.02	1.96	4.19	1.96
η (eV)	3.02	2.34	1.11	2.46	2.78	2.50
μ (eV)	−5.78	−5.04	−6.13	−4.42	−5.48	−4.46
S (eV^{-1})	0.17	0.21	0.45	0.20	0.18	0.20
ω (eV)	5.53	5.43	16.97	3.97	5.40	3.98

Table 5 Nonlinear optical values including dipole moments (μ_D), linear polarizabilities (α) and first hyperpolarizabilities (β) calculated using the PBE functional

Property	State	μ_D (Debye)	α (a.u.)	β (a.u.)	$-\Delta E$ (eV)
$B_{12}N_{12}$	—	0.00	131.1153	0.00	0
SF–$B_{12}N_{12}$	A	10.64	11.28	468.00	0
SC–$B_{12}N_{12}$	B	8.94	189.66	373.13	0
$B_{12}N_{12}$ (E_X = 0.01 a.u.)	C	0.765	1.31	8.32	0.002
SF–$B_{12}N_{12}$ (E_X = 0.01 a.u.)	D	8.56	178.10	37.47	1.382
SC–$B_{12}N_{12}$ (E_X = 0.01 a.u.)	E	6.57	191.37	239.72	1.219
$B_{12}N_{12}$ (E_Y = 0.01 a.u.)	F	0.755	131.12	8.27	0.178
SF–$B_{12}N_{12}$ (E_Y = 0.01 a.u.)	G	8.63	177.27	416.90	1.382
SC–$B_{12}N_{12}$ (E_Y = 0.01 a.u.)	H	14.43	13.74	602.82	0.979

Table 6 Effect of adsorption and external electric field on the wavenumbers of selected bonds

	Wavenumber (cm^{-1})				
Vibration	$B_{12}N_{12}$	SF	SC	SF–$B_{12}N_{12}$	SC–$B_{12}N_{12}$
B–N stretching	1379	—	—	1296	1298
P=O stretching	—	1249 (1201)[a]	1214 (1199)	1150	1105
P–C stretching	—	778	737	771	772
P–F stretching	—	684	—	823 (796)	—
P–Cl stretching	—	—	492	—	521 (480)

[a] Bracketed wavenumbers are when an external electric field is applied.

effect (QCSE).[76] The following equation can be used to estimate the relationship between the Stark shift, $-\Delta E$ and the permanent dipole moment, μ_0:

$$-\Delta E = \mu_0 F + \alpha F^2/2 + \beta F^3/6 \tag{2}$$

where the polarizability is represented as α in the direction of the electric field. The permanent dipole moments of the $B_{12}N_{12}$ fullerene interacting with SF and SC molecules were considered here and their average polarizabilities in the direction of the electric field are shown in Table 5. It was found that the Stark shift is strongly affected by the α values, which results in quadratic changes in the upper energy levels of the considered systems with an increase in the strength of the external electric field.

Recently, it has been experimentally and theoretically proven that the introduction of excess electrons into a molecule can substantially enhance its NLO parameters.[77–79] The dipole moment (μ_D) and first hyperpolarizability (β) of the bare $B_{12}N_{12}$ nanocage are equal to zero because of the uniform distribution of the charge density and therefore electronic structure, while the polarizability is reported to be 131.12 a.u.[80] The first change in the NLO values for $B_{12}N_{12}$ fullerene occurs when a molecule like SF or SC interacts with it and causes a charge transfer. This breaks the centrosymmetric electronic structure in the *ZX* plane *via* a structural deformation introduced by the lengthened B_1–N_1 bond. The application of an external electric field, especially one that is aligned with the *ZX* plane (E_Y), will further induce electrostrictive deformation in the adsorption ensemble. These changes in the non-centrosymmetric geometry and charge density distribution of the studied system will consequently affect the NLO parameters of the adsorption configurations.[81,82] The following equation describes the effect on β_{ijk} of the electron density;[83]

$$\beta_{ijk} = \int r_i {\rho_{jk}}^{(2)} \mathrm{d}r, {\rho_{jk}}^{(2)} = \frac{\partial^2 \rho}{\partial F_j \partial F_k} \tag{3}$$

where β_{ijk} is the first hyperpolarizability tensor, the superscripts *i*, *j* and *k* correspond to *x*, *y* or *z* (the Cartesian coordinates) and ρ_{jk} permutes all the indices in the expression. Therefore, any change in electron density caused by the implementation of an external electric field can affect the value of β_{ijk}.

The effects of two electric fields of E_X = 0.010 and E_Y = 0.010 a.u. on the values of μ_D, α, and β_{ijk} varied with a significant change observed for α of $B_{12}N_{12}$ upon the application of E_Y = 0.010 (131.12 a.u.). The value of the dipole moment for the bare $B_{12}N_{12}$ fullerene increased after the application of the electric fields and in the case of SF/SC–$B_{12}N_{12}$ it again revealed a decrease, except for the state H (Table 4). The value of α for the bare $B_{12}N_{12}$ fullerene decreased significantly upon the application of the electric field in the *X* direction, while the interaction of SC and SF with $B_{12}N_{12}$ again increases this value. This suggests that the polarizability of the $B_{12}N_{12}$ fullerene is significantly affected by both the application of the electric field and the interactions of SC and SF towards the $B_{12}N_{12}$ fullerene. The first hyperpolarizability value also changed from 0.00 a.u. for the bare $B_{12}N_{12}$ fullerene to 8.32 and 8.27 a.u. due to the application of electric fields through the +*X* and +*Y* directions, respectively. The value of β for the bare $B_{12}N_{12}$ fullerene also increased significantly due to interactions with SC and SF and then decreased after the application of electric fields in the *X* and *Y* directions; the exception is for state H, in which the value of β increased. Li *et al.*[84] reported on the application of external electric fields to hydrogenated silicon nanoclusters (H-SiNCs) and their possible effects on the NLO parameters of the H-SiNCs. They found that the second hyperpolarizability increased upon the application of electric fields from all three directions of *X*, *Y* and *Z*, which is in agreement with our NLO results. They believe that the electron density distribution changes owing to the electric fields and becomes more polarized, resulting in the higher values for the NLO parameters.[83,85]

Moreover, the results of the main electron transitions for different electronic states (Table 5) provide further evidence for the idea that the application of external electric fields can change the electronic structure of adsorption systems. This is owing to electron transfer from different HOMO levels to different LUMO levels and even the percentage contributions of each main transition change upon the application of electric fields, which is more obvious in the case of E_Y compared to that of E_X. As discussed by Wang *et al.*, the application of a small amount of electric field may cause a big change in the value of β.[86] The application of electric fields of E_Y = 0.010 a.u. and E_X = 0.010 a.u. reduces the value of β for states G, F and H, while it increases the value of β for the C configuration. Most likely, our study follows similar behaviour as reported by Li[84] and Wang.[86] Generally, as it is clear from the bond lengths and bond angles, important changes occur as a result of the application of external electric fields. Moreover, the shapes of the lobes of the

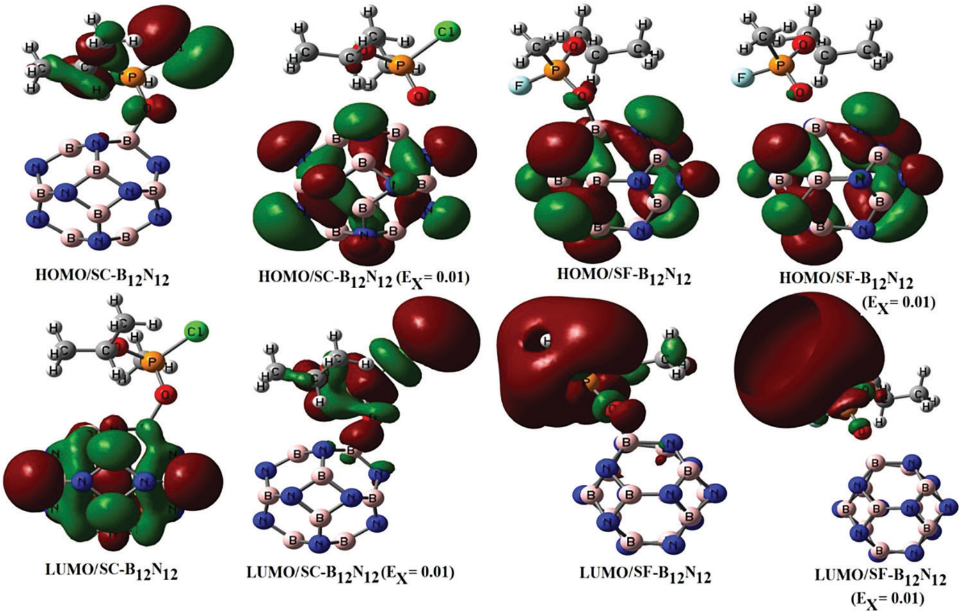

HOMO/SC-$B_{12}N_{12}$ HOMO/SC-$B_{12}N_{12}$ (E_X = 0.01) HOMO/SF-$B_{12}N_{12}$ HOMO/SF-$B_{12}N_{12}$ (E_X = 0.01)

LUMO/SC-$B_{12}N_{12}$ LUMO/SC-$B_{12}N_{12}$ (E_X = 0.01) LUMO/SF-$B_{12}N_{12}$ LUMO/SF-$B_{12}N_{12}$ (E_X = 0.01)

Fig. 5 HOMO and LUMO orbitals of SF and SC molecules adsorbed on $B_{12}N_{12}$ fullerene.

occupied and unoccupied molecular orbitals changed significantly before and after electric field application (Fig. 5). Under an external electric field, the HOMO and LUMO were redistributed along the direction of the electric field by forming a dipole in that direction. These results reveal that the electric field not only affects the geometry and structural parameters of the adsorption configurations but also changes the electron density distribution of the systems as it eventually results in significant changes in the NLO parameters.

3.5. Electronic properties

The molecular orbital energies (MOEs) represent the properties of the excited states by providing an insight into the absorption spectra of the SF/SC–$B_{12}N_{12}$ interaction configurations. Table 3 shows the decrease in the difference between the HOMO and LUMO states (E_g) when a uniform external electric field was applied. Under an electric field, the dipole realignment of the HOMO and LUMO along the direction of the electric field occurred to occupy a lower energy level and more stable state. The LUMO experiences a greater energy reduction as it is empty while the HOMO has a higher local charge density. This trend of decreasing HOMO–LUMO gap under increasing field strengths would then cause a decrease in the effective work function. The theoretical results reveal that the E_g value for $B_{12}N_{12}$ determined using the PBE functional in comparison with the B3LYP (E_g = 6.71 eV) and M06-2X (E_g = 7.20 eV) methods is in good agreement with experimental data for $B_{12}N_{12}$ determined by Oku *et al.* (E_g = 5.1 eV).[25] The HOMO–LUMO difference (E_g) for the bare $B_{12}N_{12}$ fullerene was calculated to be 4.99 eV while it is 4.47 and 3.74 eV for the respective SF–$B_{12}N_{12}$ and SC–$B_{12}N_{12}$ interaction configurations. The interaction of SF and SC with $B_{12}N_{12}$ resulted in more molecular orbitals being formed in both the SF–$B_{12}N_{12}$ and SC–$B_{12}N_{12}$ adsorption systems. These additional molecular orbitals contributed to the additional new states as detected in the total density of state (TDOS) and PDOS spectra of the adsorption systems (Fig. 6). In the formation of such molecular orbitals, it has also been observed that the energies of HOMO and LUMO were respectively increased and decreased during adsorption, causing a decrease in the HOMO–LUMO energy gap of 10.4% and 25.1% for the SF–$B_{12}N_{12}$ and SC–$B_{12}N_{12}$ systems, respectively (Table 1). Such decreases will enable easier electronic transitions in the SF–$B_{12}N_{12}$ and SC–$B_{12}N_{12}$ systems, as shown in the bathochromic shifts of $\lambda_{\max}$ for the UV-vis excitation of these adsorption systems (Table 7).

The E_g for $B_{12}N_{12}$ under two applied external electric fields changed in accordance with the strength of the applied electric field, with the greatest change observed for E_Y =0.010 a.u. Moreover, the E_F only experienced moderate changes, except for the case of E_Y = 0.005 (Table 2). For the adsorption of SF and SC on the $B_{12}N_{12}$ fullerene in the presence of an electric field, the changes to E_g are more noticeable in the presence of E_X = 0.010 a.u. The ΔE_g (%) consequently underwent greater changes in the same manner as E_g. The value of E_g in the presence of E_X = 0.010 a.u. reduced significantly from 4.76 eV to 2.21 and 2.51 eV for the respective SF–$B_{12}N_{12}$ and SC–$B_{12}N_{12}$ systems while these changes were weaker in the presence of E_Y = 0.010 a.u. Therefore, the decrease in E_g for both systems under a strong parallel electric field leads to a reduction in stability and an increase in chemical reactivity, while such effects were reduced in the case of a perpendicular electric field.[87–90] In the case of E_F and μ_D, the reverse is observed, where more significant changes happen in the presence of E_Y = 0.005 and 0.010 a.u. (Table 3).

Fig. 6 shows the TDOS, PDOS, and space overlap population density of states (OPDOS) for SC and SF interacting with the $B_{12}N_{12}$ fullerene. The remarkable phenomenon that can be observed in the figure is the directional electric field anisotropy

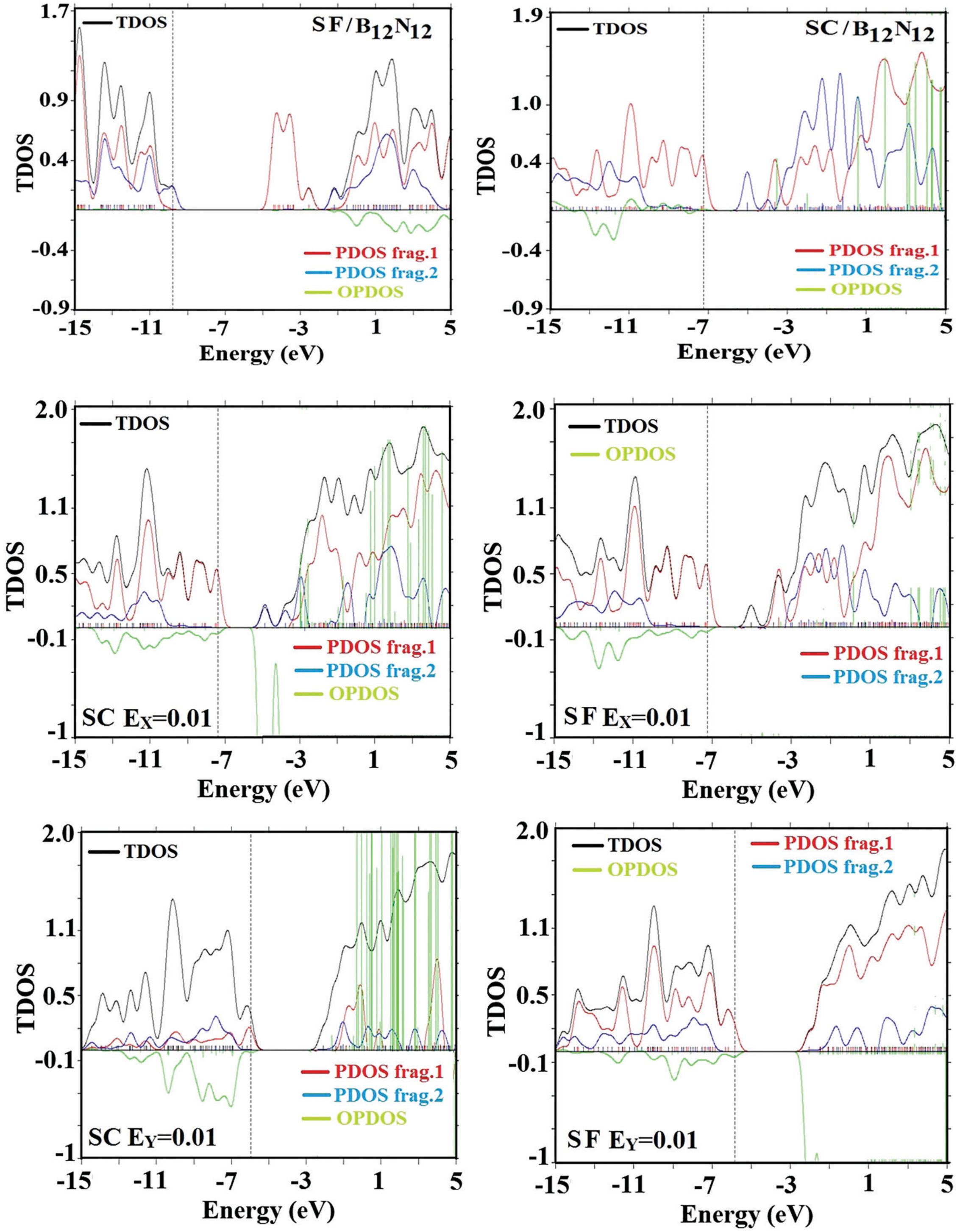

Fig. 6 TDOS and PDOS plots for the $B_{12}N_{12}$ fullerene interacting with SC and SF molecules.

and the associated change in the electronic structure of the system. It is clear that, in the presence of an external electric field, some new states appeared and there are some broken degeneracies in the filled occupied and unoccupied states for the systems that are attributed to the Stark effect. The change is related to the HOMO and LUMO states and the quantum states near the band edges. It can be seen that upon the interaction of SC or SF with the $B_{12}N_{12}$ fullerene that the E_g can increase or decrease depending on the electric field direction. When the electric field is applied along the $+X$ direction, the HOMO–LUMO gap increases with the increment of the field strength while the reverse situation results with the electric field along the $+Y$ direction.

The electric field can also influence the OPDOS of the system. In comparison with the isolated $B_{12}N_{12}$ molecule, the

Table 7 Selected excitation energies (E), oscillator strengths (f), wavelengths (λ_{max}), and relative orbital contributions calculated using the PBE functional

Structure	E (eV)	f	λ_{max} (nm)	Main transitions
$B_{12}N_{12}$	6.05	0.0001	205	H−1 → L+1 (75%), H → L+2 (12%)
	6.06	0.0001	204	H−2 → L+2 (42%), H → L+2 (33%)
	6.07	0.0001	204	H−2 → L+1 (18%), H−2 → L+3 (27%)
SF–$B_{12}N_{12}$	5.70	0.0110	217	H−5 → LUMO (24%), H−4 → L+1 (20%), H−4 → L+2 (30%)
	5.53	0.0074	223	H−3 → LUMO (93%), HOMO → L+7 (4%)
	5.11	0.0059	242	HOMO → L+4 (87%), H−1 → L+3 (6%)
SC–$B_{12}N_{12}$	5.57	0.0104	222	H−9 → LUMO (30%), H−3 → L+1 (24%), H−2 → L+5 (16%)
	4.44	0.0166	279	H−3 → LUMO (100%)
	3.71	0.0079	334	HOMO → LUMO (100%)
$B_{12}N_{12}$ (E_X = 0.01 a.u.)	5.79	0.0245	214	H−5 → LUMO (45%), HOMO → L+5 (16%)
	5.61	0.0010	220	H−1 → L+3 (42%), H−1 → L+4 (42%)
	4.96	0.0007	249	H−2 → LUMO (11%), H−1 → L+1 (89%)
SF–$B_{12}N_{12}$ (E_X = 0.01 a.u.)	5.75	0.0273	215	H−5 → L+2 (10%), H−1 → L+7 (22%), HOMO → L+8 (24%)
	5.58	0.0053	222	H−3 → L+1 (71%), H−4 → LUMO (3%)
	5.15	0.0122	240	H−1 → L+3 (98%)
SC–$B_{12}N_{12}$ (E_X = 0.01 a.u.)	5.56	0.0049	222	H−1 → L+5 (22%), HOMO → L+7 (51%)
	5.18	0.0031	239	H−6 → LUMO (99%)
	4.61	0.0212	261	H−3 → LUMO (97%)
$B_{12}N_{12}$ (E_Y = 0.01 a.u.)	5.78	0.0245	214	H−4 → LUMO (45%), H−4 → L+1 (15%), H−1 → L+5 (12%)
	5.67	0.0029	218	H−3 → L+2 (16%), H−2 → L+4 (58%)
	4.98	0.0006	248	H−2 → L+1 (85%), H−1 → L+1 (9%)
SF–$B_{12}N_{12}$ (E_Y = 0.01 a.u.)	5.73	0.0139	216	H−5 → L+1 (11%), H−5 → L+2 (16%), H−1 → L+7 (12%)
	5.43	0.0023	228	H−2 → L+3 (15%), HOMO → L+4 (51%), HOMO → L+6 (22%)
	4.89	0.0023	253	H−1 → L+2 (86%), H−2 → LUMO (5%), H−1 → L+1 (7%)
SC–$B_{12}N_{12}$ (E_Y = 0.01 a.u.)	5.25	0.0157	236	H−10 → LUMO (81%), H−1 → L+5 (15%)
	4.75	0.0068	261	HOMO → L+2 (100%)
	3.94	0.0044	314	H−4 → LUMO (100%)

electric field along the +X and +Y directions changes the OPDOS values, especially near the HOMO and LUMO states. The negative values for the OPDOS show the anti-bonding nature (with green color) of the interaction between the examined molecules and the host fullerene, which is significantly below the Fermi level, while the positive values show the bonding states, which are above the LUMO state. The electric field switches the anti-bonding states to the bonding state for the SC and SF interacting with the $B_{12}N_{12}$ fullerene, providing more vacant orbitals on the $B_{12}N_{12}$ fullerene for possible interaction with SC or SF molecules.

3.6. Quantum molecular descriptor analysis

In the absence of an external electric field, the ionization potential (I = 7.03 eV) for the bare $B_{12}N_{12}$ corresponds to the high stability and chemical inertness of the fullerene, which decreases after adsorption with I = 5.93 eV for SF–$B_{12}N_{12}$ and I = 6.01 eV for SC–$B_{12}N_{12}$.[91] The hardness (η) and softness (S) of the SF–$B_{12}N_{12}$ and SC–$B_{12}N_{12}$ systems experienced decreasing and increasing trends, respectively, which is in accordance with the reduction of E_g for $B_{12}N_{12}$ fullerene after interactions with both molecules. These results imply that the polarization of $B_{12}N_{12}$ fullerene is reduced as a result of the interaction with SF and SC molecules. The dipole moment (μ_D) for $B_{12}N_{12}$ fullerene is zero, indicating the uniform distribution of electron density,[91] which increased after adsorption for these two systems, causing deformation and at the same time facilitating the adsorption behavior with a greater μ_D for SF–$B_{12}N_{12}$ (10.71 Debye) than SC–$B_{12}N_{12}$ (9.18 Debye).[92] The value of the electrophilicity index (ω) indicates that the $B_{12}N_{12}$ fullerene functions as a nucleophile (electron donor) but changes to an electrophile (electron acceptor) in the SF–$B_{12}N_{12}$ and SC–$B_{12}N_{12}$ systems.

The corresponding global indices for the bare $B_{12}N_{12}$ fullerene changed after inclusion of the four electric fields of E_X = 0.005, 0.010 a.u. and E_Y = 0.005, 0.010 a.u., with the largest changes observed for the +X direction with a strength of 0.010 a.u. Upon adsorption of SF and SC in the presence of the applied electric fields, the ionization potential (I) decreases, particularly for E_Y = 0.010 a.u., indicating greater reactivity of $B_{12}N_{12}$ towards SF and SC molecules. The adsorption systems showed the highest and lowest electron affinities under external electric fields of E_X = 0.010 and E_Y = 0.005 a.u., respectively.[93,94] In accordance with the lowering of the E_g values, the hardness and softness of the SF–$B_{12}N_{12}$ and SC–$B_{12}N_{12}$ systems changed under an electric field compared to the bare $B_{12}N_{12}$ structure, implying that the resistance and polarization of $B_{12}N_{12}$ fullerene have decreased. The reactivity of the systems increased linearly with the electric field strength with the effect generated by the application of E_X = 0.010 a.u. being greater than that seen for the other applied fields. The μ_D values for E_Y = 0.005, 0.010 a.u. were more noticeable than other fields, which appreciably confirms the adsorption values obtained for these systems and their degree of deformability. The ω values show the more nucleophilic nature (electron donation) with an electric field of E_Y = 0.005 a.u. and the more electrophilic nature (electron acceptance) with an electric field of E_X = 0.010 a.u. for $B_{12}N_{12}$ after the interactions.

3.7. Electron density and localized orbital locator

Fig. 7 and 8 show the color-filled electron density plots for the pure $B_{12}N_{12}$ fullerene and the $B_{12}N_{12}$ fullerene after interacting with SF and SC molecules. The electron densities for SF and SC

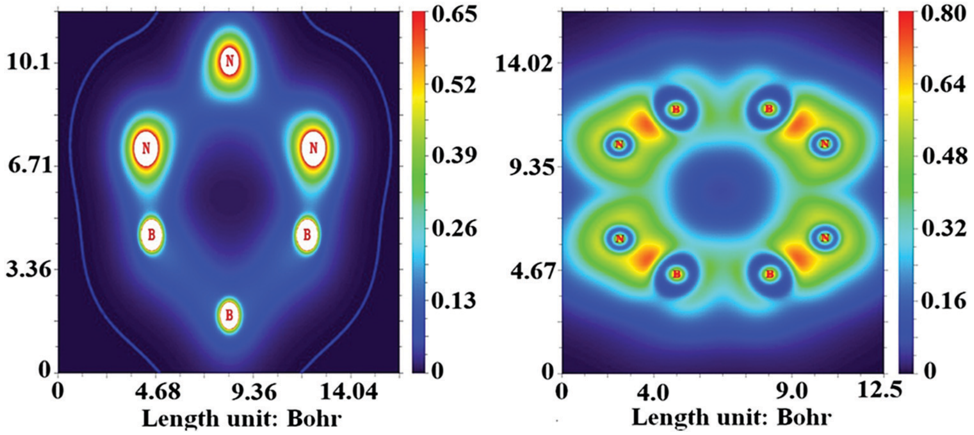

Fig. 7 Color-filled electron density maps and localized orbital locator of pure $B_{12}N_{12}$ fullerene under E_X = 0.01 a.u.

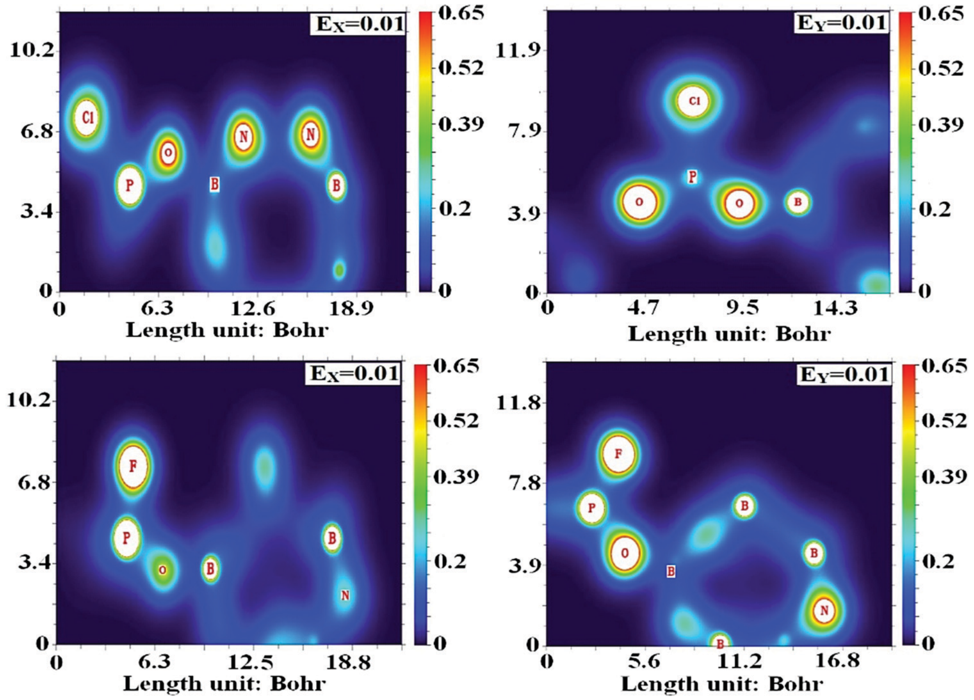

Fig. 8 Color-filled electron density maps for $B_{12}N_{12}$ fullerene interacting with SC (top panels) and SF (down panels) molecules under E_X = 0.01 a.u. and E_Y = 0.01 a.u.

adsorbed on the B atom of the $B_{12}N_{12}$ fullerene were calculated for E_X = 0.010 and E_Y = 0.010 a.u. There is an apparent charge transfer occurring from the molecules to the $B_{12}N_{12}$ fullerene near the interaction sites, which is the consequence of strong chemical interactions[95] for E_Y (Fig. 8). This result is in agreement with the MPA results. Fig. 9 includes the localized orbital locator (LOL) plot of a small part of the $B_{12}N_{12}$ fullerene where the isovalue of the contour line is 0.5. As displayed in Fig. 9, the polar covalent B–O bonds in the SF–$B_{12}N_{12}$ and SC–$B_{12}N_{12}$ complexes for E_Y = 0.010 a.u. exhibit stronger chemical bonding through their larger orbital localizations with the region of relatively large LOL values.[96,97]

3.8. Infrared analysis

The adsorption of SF and SC on $B_{12}N_{12}$ fullerene was investigated to evaluate the changes in the infrared (IR) spectral characteristics using the PBE functional (Fig. S2, ESI†). The Gaussian program follows the calculation method of Komornicki and McIver[98] for the integrated IR intensities associated with each vibrational mode. In this study, a scaling factor of 0.975 was employed from the PBE functional. The vibrational frequencies of the $B_{12}N_{12}$ fullerene range from 312 to 1416 cm^{-1} with the B–N stretching vibration in the pure $B_{12}N_{12}$ fullerene being located at around 1379 cm^{-1},[99] decreasing to 1298 cm^{-1} for SC–$B_{12}N_{12}$ and 1296 cm^{-1} for SF–$B_{12}N_{12}$. Anota *et al.*[100]

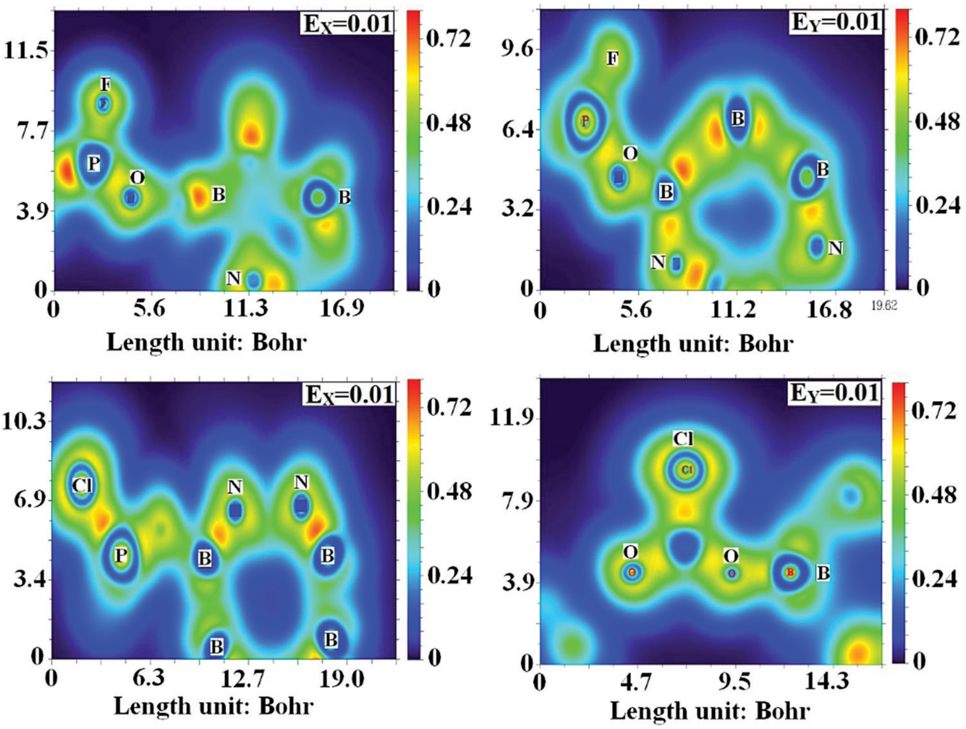

Fig. 9 Localized orbital locator plots for $B_{12}N_{12}$ fullerene interacting with SF (top panels) and SC (down panels) molecules under E_X = 0.01 a.u. and E_Y = 0.01 a.u.

theoretically presented the vibrational bands of B–N and N–N in $B_{24}N_{36}$ fullerene at around 1473.0, 1511.0, 1536.7 and 1557.2 cm^{-1}. In a study by Shin *et al.*,[101] the peaks in the IR spectrum of the pristine BNNTs are reported as the in-plane B–N stretching and the out-of-plane B–N–B bending modes observed at 1383 and 806 cm^{-1}, respectively. The bands at 1249 and 778 cm^{-1} are assigned to P═O and P–C stretching vibrations in the SF molecule, while for the SC molecule these bands are observed at around 1214 and 737 cm^{-1}, respectively.[102] In the presence of an electric field, the adsorbed P═O stretching mode bands decreased to 1201 and 1199 cm^{-1} in the SF–$B_{12}N_{12}$ and SC–$B_{12}N_{12}$ complexes, respectively. The experimental IR data indicated that the adsorbed P═O stretching mode is at 1250 cm^{-1} with measurable intensity.[103] Mott and Rez experimentally demonstrated that the P═O stretching vibration of sarin was at 1308 cm^{-1}, which is in agreement with our results.[104] The P═O and P–C stretching vibrations are observed at 1150 and 771 cm^{-1} for SF–$B_{12}N_{12}$ and at 1105 and 772 cm^{-1} for SC–$B_{12}N_{12}$, respectively. The formation of a B···O═P bond during adsorption weakens the covalent bonding of P═O and B–N bonds, causing their vibration frequencies to decrease.

The bands located at 684 and 492 cm^{-1} correspond to the P–F and P–Cl stretching vibrations for SF and SC, respectively.[105] The IR spectral change for SC–$B_{12}N_{12}$ is similar to that for SF–$B_{12}N_{12}$ and the peaks at around 823 and 521 cm^{-1} are assigned to the P–F and P–Cl stretching vibrations in SF–$B_{12}N_{12}$ and SC–$B_{12}N_{12}$, respectively.[106,107] In the presence of an electric field, the P–F and P–Cl stretching vibrations for SF and SC adsorbed on $B_{12}N_{12}$ fullerene decreased to 796 and 480 cm^{-1}, respectively. P–F and P–Cl bonds are non-chemisorbed bonds during the adsorption. The weakened P═O bond will enhance the mesomeric effect within F–P═O and Cl–P═O through the donation of a lone pair of electrons by F and C onto P to stabilize the P═O bond. This mesomeric effect increases the polar character of the P–F and P–Cl bonds, making them stronger and thus having higher vibration frequencies. This effect was more significant in the P–F bond as F is smaller than Cl, enabling a greater overlapping of its valence p orbital with the π-orbital of the P═O bond. The overall decrease in the vibrational frequencies under an external electric field is attributed to the energy downshift by the Stark effect (Table 6). Therefore, our results indicate that the $B_{12}N_{12}$ fullerene under an electric field exhibits the largest change in the vibrational spectrum.

3.9. UV-vis analysis

Excited state TDDFT calculations were performed on the isolated $B_{12}N_{12}$ and the SF/SC–$B_{12}N_{12}$ fullerenes with and without an external electric field using the PBE functional (Table 7). The ultraviolet-visible (UV-vis) spectrum of the pure $B_{12}N_{12}$ fullerene shows three very weak main peaks at 205, 204 and 204 nm with energies of 6.05, 6.06 and 6.07 eV for the main electron transitions, respectively (Fig. S3, ESI†).[108–110] We also calculated the exciton binding energy (E_b) for the pure $B_{12}N_{12}$ fullerene to be −1.06 eV, while in the parallel and perpendicular electric fields it was found to be −0.25 and −0.87 eV, respectively. A suspension of BN nanotubes in ethanol shows a broad UV absorbance reaching a maximum at 207 nm with an optical band gap of 5.9 eV,[111,112] which is close to our results calculated using the PBE functional. After the interaction of SF and SC toxic agents, through nucleophilic attack of oxygen, with the boron atom of the $B_{12}N_{12}$ fullerene, the main absorption peaks are red-shifted to higher wavelengths (λ_{max}) at 217 nm (SF–$B_{12}N_{12}$) and 279 nm (SC–$B_{12}N_{12}$) with lower energies of 5.70 and 4.44 eV and oscillator strengths (f) of 0.0110 and 0.0166, respectively.

The main electron transitions changed with the transitions occurring from H−4 to L+2 (30%) in SF–$B_{12}N_{12}$ and H−3 to LUMO (100%) in SC–$B_{12}N_{12}$ compared to H−1 to L+1 (75%) for pure $B_{12}N_{12}$ fullerene. For SF and SC interacting with the $B_{12}N_{12}$ fullerene, the values of E_b were −1.23 and −0.7 eV, changing to −3.54 and −2.1 eV in the parallel electric field and −1.91 and −1.37 eV in the perpendicular electric field, respectively. The absorption peaks for the main electron transitions changed significantly for the adsorption configurations with the external electric fields in the directions of $+X$ and $+Y$. The application of an external electric field in the $+X$ direction causes more changes within the absorption spectra. The main electron transitions in the UV-vis spectra for the adsorption configurations in the presence of the parallel electric field occur from the HOMO (H) to L+8 (24%) in SF–$B_{12}N_{12}$ and H−3 to the LUMO (97%) in SC–$B_{12}N_{12}$, changing appreciably to different HOMO and LUMO levels upon the application of an external electric field to the adsorption systems. The increase in the electron transfers between the bonding and anti-bonding energy levels owing to the application of the external electric field, especially in the $+X$ direction, may be the key reason for the increase in the maximum wavelengths (λ_{max}) in the interaction between the toxic agents and the $B_{12}N_{12}$ fullerene.

4. Conclusions

To summarize, DFT and TDDFT calculations were performed to explore the adsorption of SF and SC molecules on $B_{12}N_{12}$ fullerene, with and without an electric field. The calculations demonstrate that SF and SC molecules can be chemisorbed upon the walls of $B_{12}N_{12}$ fullerene, resulting in notable adsorption energies and charge transfer, inducing significant changes in the structural properties of the fullerenes. It was also found that the adsorption of SF–$B_{12}N_{12}$ and SC–$B_{12}N_{12}$ in the presence of an electric field in the $+Y$ direction is more significant than that in the $+X$ direction or without an electric field, suggesting that the $B_{12}N_{12}$ fullerene has a strong binding energy in the $+Y$ direction with the SF and SC molecules. The calculations also reveal that $B_{12}N_{12}$ has greater sensitivity for the detection of SF in the $+X$ direction (E_X = 0.010 a.u.) compared with SC. The electric field switches the anti-bonding states to the bonding state for SC and SF interacting with $B_{12}N_{12}$ fullerene. This increases the number of available positions on the $B_{12}N_{12}$ fullerene for the stable adsorption of SC or SF molecules. Therefore, the results demonstrate the enhancement of SF and SC detection and sensing in the presence of a parallel electric field compared to in the presence of a perpendicular electric field. A parallel electric field results in greater changes to the energy gap and the electrical conductivity of the adsorbent and visible shifts in the UV-vis spectra, which all facilitate the development of sensors for the toxic agents SF and SC.

Conflicts of interest

There are no conflicts to declare.

Acknowledgements

We would like to thank the Clinical Research Development Unit (CRDU), Sayad Shirazi Hospital, Golestan University of Medical Sciences, Gorgan, Iran. We would like to thank Golestan University, Gorgan, Iran. Mohammad Ramezanitaghartapeh acknowledges the SUPRA scholarship provided by Swinburne University of Technology.

References

1 W. Kroto, J. R. Heath, S. C. O'Brien, R. F. Curl and R. E. Smalley, *Nature*, 1985, **318**, 162.
2 E. Neyts, A. Maeyens, G. Pourtois and A. Bogaerts, *Carbon*, 2011, **49**, 1013.
3 Y. X. Ren, T. Y. Ng and K. M. Liew, *Carbon*, 2006, **44**, 397.
4 A. Ahmadi, N. L. Hadipour, M. Kamfiroozi and Z. Bagheri, *Sens. Actuators, B*, 2012, **161**, 1025.
5 F.-L. Liu and C.-H. Wang, *Spectrochim. Acta, Part A*, 2008, **70**, 1141.
6 J. Beheshtian, A. Ahmadi Peyghan and Z. Bagheri, *Comput. Mater. Sci.*, 2012, **62**, 71.
7 Q. Wang, Q. Sun, P. Jena and Y. Kawazoe, *J. Am. Chem. Soc.*, 2009, **3**, 621.
8 W. Y. Ching, M. Zh, M. Zh. Huang, Y. N. Xu, W. G. Harter and F. T. Chan, *Phys. Rev. Lett.*, 1991, **67**, 2045.
9 J. L. Li, Y. Y. Xia, M. W. Zhao, X. D. Liu, C. Song, L. J. Li, F. Li and B. D. Huang, *J. Phys.: Condens. Matter*, 2007, **19**, 346228.
10 A. Costales, M. A. Blanco, E. Francisco, R. Pandey and A. M. Pendas, *J. Phys. Chem. B*, 2005, **109**, 24352.
11 A. V. Pokropivny, *Diamond Relat. Mater.*, 2006, **15**, 1492.
12 A. Ahmadi, M. Pshanpour, Z. Bagheri and M. Kamfiroozi, *Physica E*, 2012, **44**, 1436.
13 J. M. L. Martin, J. El-Yazal, J.-P. Francois and R. Gijbels, *Chem. Phys. Lett.*, 1995, **232**, 289.
14 J. M. L. Martin, J. El-Yazal and J.-P. Francois, *Chem. Phys. Lett.*, 1996, **248**, 95.
15 D. L. Strout, *J. Phys. Chem. A*, 2000, **104**, 3364.
16 D. L. Strout, *J. Phys. Chem. A*, 2001, **105**, 261.
17 H. S. Wu, X. Y. Cui, X. F. Qin, D. L. Strout and H. Jiao, *J. Mol. Model.*, 2006, **12**, 537.
18 N. G. Chopra, *et al.*, *Science*, 1995, **269**, 966.
19 D. Golberg, Y. Bando, O. St_ephan and K. Kurashima, *Appl. Phys. Lett.*, 1998, **73**, 2441.
20 D. Golberg, Y. Bando, K. Kurashima and T. Sato, *Scr. Mater.*, 2001, **44**, 1561.

21 D.-B. Zhang, E. Akatyeva and T. Dumitrica, *Phys. Rev. B: Condens. Matter Mater. Phys.*, 2011, **84**, 115431.

22 D. L. Strout, *Chem. Phys. Lett.*, 2004, **383**, 95–98.

23 A. Soltani, S. Ghafouri Raz, M. Ramezani Taghartapeh, A. Varasteh Moradi and R. Zafar Mehrabian, *Comput. Mater. Sci.*, 2013, **79**, 795–803.

24 B. Peles-Lemli, D. Kánnár, J.-C. Nie, H. Li and S. Kunsagi-Mate, *J. Phys. Chem. C*, 2013, **117**(41), 21509–21515.

25 T. Oku, A. Nishiwaki and I. Narita, *Sci. Tech. Adv. Mater.*, 2004, **5**, 635–638.

26 P. Matvija, F. Rozbořil, P. Sobotík, I. Oštádal, B. Pieczyrak, L. Jurczyszyn and P. Kocán, *Sci. Rep.*, 2017, **7**, 7357.

27 R. Q. Zhang, C. Hou, N. Gao, Z. Wen and Q. Jiang, *Chem. Phys. Chem.*, 2011, **12**, 1302–1309.

28 Y. Li, S. V. Rotkin and U. Ravaioli, *Nano Lett.*, 2003, **3**, 183–187.

29 W. Liu, Y. H. Zhao, Y. Li, E. J. Lavernia and Q. Jiang, *Phys. Chem. Chem. Phys.*, 2009, **11**, 9233–9240.

30 W. Liu, Y. H. Zhao, J. Nguyen, Y. Li, Q. Jiang and E. J. Lavernia, *Carbon*, 2009, **47**, 3452–3460.

31 E. V. Castro, K. S. Novoselov, S. V. Morozov, N. M. R. Peres, J. M. B. L. dos Santos, J. Nilsson, F. Guinea, A. K. Geim and A. H. Castro Neto, *Phys. Rev. Lett.*, 2007, **99**, 216802.

32 K. S. Novoselov, A. K. Geim, S. V. Morozov, D. Jiang, Y. Zhang, S. V. Dubonos, I. V. Grigorieva and A. A. Firsov, *Science*, 2004, **306**, 666–669.

33 T. Mitsui, E. Fomin, D. F. Ogletree, M. Salmeron, A. U. Nilekar and M. Mavrikakis, *Angew. Chem., Int. Ed.*, 2007, **46**, 5757–5761.

34 H. Liu and J. Y. Lee, *J. Phys. Chem. C*, 2012, **116**, 3034–3041.

35 S. Sriram, M. Bhaskaran, S. Chen, S. Jayawardhana, P. R. Stoddart, J. Z. Liu, N. V. Medhekar, K. Kalantar-Zadeh and A. Mitchell, *J. Am. Chem. Soc.*, 2012, **134**, 4646–4653.

36 C. F. Gorin, E. S. Beh, Q. M. Bui, G. R. Dick and M. W. Kanan, *J. Am. Chem. Soc.*, 2013, **135**(30), 11257–11265.

37 J. Kassa, M. Pecka, M. Tichy, J. Bajgar, M. Koupilova, J. Herink and Z. Krocova, *Pharmacol. Toxicol.*, 2001, **88**, 209–212.

38 J.-M. Collombet, F. Mourcin, N. Grenier, E. Four, C. Masqueliez, D. Baubichon, G. Lallement and F. Herodin, *NeuroToxicology*, 2005, **26**, 89–98.

39 A. W. Abu-Qare and M. B. Abou-Donia, *Toxicol. Lett.*, 2001, **123**, 51–58.

40 V. M. Bermudez, *J. Phys. Chem. C*, 2007, **111**, 9314–9323.

41 A. Michalkova, M. Ilchenko, L. Gorb and J. Leszczynski, *J. Phys. Chem. B*, 2004, **108**, 5294–5303.

42 C. J. O'Brien, J. A. Greathouse and C. M. Tenney, *J. Phys. Chem. C*, 2016, **120**, 28100–28109.

43 S. M. Kanan, Z. Lu and C. P. Tripp, *J. Phys. Chem. B*, 2002, **106**, 9576–9580.

44 B. N. Papas, I. D. Petsalakis, G. Theodorakopoulos and J. L. Whitten, *J. Phys. Chem. C*, 2014, **118**, 23042–23048.

45 A. Soltani, M. T. Baei, M. Ramezani Taghartapeh, E. Tazikeh Lemeski and S. Shojaee, *Struct. Chem.*, 2015, **26**, 685–693.

46 M. T. Baei, A. S. Ghasemi, E. Tazikeh Lemeski, A. Soltani and N. Gholami, *J. Cluster Sci.*, 2016, **27**, 1081–1096.

47 H. Liu and J. Y. Lee, *J. Phys. Chem. C*, 2012, **116**, 3034–3041.

48 M. J. Frisch, G. W. Trucks, H. B. Schlegel, G. E. Scuseria, M. A. Robb, J. R. Cheeseman, G. Scalmani, V. Barone, B. Mennucci, G. A. Petersson, H. Nakatsuji, M. Caricato, X. Li, H. P. Hratchian, A. F. Izmaylov, J. Bloino, G. Zheng, J. L. Sonnenberg, M. Hada, M. Ehara, K. Toyota, R. Fukuda, J. Hasegawa, M. Ishida, T. Nakajima, Y. Honda, O. Kitao, H. Nakai, T. Vreven, J. A. Montgomery, Jr., J. E. Peralta, F. Ogliaro, M. Bearpark, J. J. Heyd, E. Brothers, K. N. Kudin, V. N. Staroverov, R. Kobayashi, J. Normand, K. Raghavachari, A. Rendell, J. C. Burant, S. S. Iyengar, J. Tomasi, M. Cossi, N. Rega, J. M. Millam, M. Klene, J. E. Knox, J. B. Cross, V. Bakken, C. Adamo, J. Jaramillo, R. Gomperts, R. E. Stratmann, O. Yazyev, A. J. Austin, R. Cammi, C. Pomelli, J. W. Ochterski, R. L. Martin, K. Morokuma, V. G. Zakrzewski, G. A. Voth, P. Salvador, J. J. Dannenberg, S. Dapprich, A. D. Daniels, Ö. Farkas, J. B. Foresman, J. V. Ortiz, J. Cioslowski and D. J. Fox, *Gaussian 09, Revision A.1*, Gaussian, Inc., Wallingford, CT, 2009; J. P. Perdew, K. Burke and M. Ernzerhof, *Phys. Rev. Lett.*, 1996, **77**, 3865.

49 A. D. Becke, *J. Chem. Phys.*, 1993, **98**, 5648.

50 T. C. Lee, W. T. Yang and R. G. Parr, *Phys. Rev. B: Condens. Matter Mater. Phys.*, 1988, **7**, 785.

51 Y. Zhao and D. G. Truhlar, *Theor. Chem. Acc.*, 2008, **120**, 215–241.

52 M. Bezi Javan, A. Soltani, E. Tazikeh Lemeski, A. Ahmadi and S. Moazen Rad, *Superlattices Microstruct.*, 2016, **100**, 24–37.

53 Z. Ma, Y. Zhang, F. Li and H. Chen, *Comput. Mater. Sci.*, 2016, **117**, 71–75.

54 A. Mohajeri and M. Ebadi, *J. Phys. Chem. A*, 2012, **116**, 4678–4686.

55 D. L. Strout, *Chem. Phys. Lett.*, 2004, **383**, 95–98.

56 J. M. Matxain, L. A. Eriksson, J. M. Mercero, X. Lopez, M. Piris, J. M. Ugalde, J. Poater, E. Matito and M. Sola, *J. Phys. Chem. C*, 2007, **111**, 13354–13360.

57 Q. Wang, M.-H. Wang, X. Lu, K.-F. Wang and L.-M. Fang, *Chem. Phys. Lett.*, 2017, **685**, 385–394.

58 D. Farmanzadeh and S. Ghazanfary, *Appl. Surf. Sci.*, 2014, **320**, 391–399.

59 Y. C. Quintero and R. Nagarajan, *Surf. Sci.*, 2018, **675**, 26–35.

60 A. Rodríguez Juárez, M. Salazar Villanueva, D. Cortés-Arriagada and E. Chigo Anota, *J. Mol. Model.*, 2019, **25**, 21.

61 S. Okada and A. Oshiyama, *Chem. Phys. Lett.*, 2005, **414**, 429.

62 A. Freitas, S. Azevedo and J. R. Kaschny, *Solid State Commun.*, 2013, **153**, 40–45.

63 J. Beheshtian, Z. Bagheri, M. Kamfiroozi and A. Ahmadi, *Microelectron. J.*, 2011, **42**, 1400–1403.

64 A. Soltani and M. Bezi Javan, *RSC Adv.*, 2015, **5**, 90621–90631.

65 M. T. Baei, A. Ahmadi Peyghan and Z. Bagheri, *Bull. Korean Chem. Soc.*, 2012, **33**, 3338–3342.

66 M. T. Baei, M. Ramezani Taghartapeh, E. Tazikeh Lemeski and A. Soltani, *Physica B*, 2014, **444**, 6–13.

67 M. D. Ganji, H. Yazdani and A. Mirnejad, *Physica E*, 2010, **42**, 2184–2189.

68 V. M. Bermudez, *J. Phys. Chem. C*, 2009, **113**, 1917–1930.

69 Y. Yamini and M. Moradi, *Sens. Actuators, B*, 2014, **197**, 274–279.

70 J. Beheshtian, A. Ahmadi Peyghan and Z. Bagheri, *Sens. Actuators, B*, 2012, **171–172**, 846–852.

71 M. Razmkhah, M. T. H. Mosavian, F. Moosavi and A. Ahmadpour, *Appl. Surf. Sci.*, 2018, **456**, 318–327.

72 T. Kuila, S. Bose, P. Khanra, A. K. Mishra, N. H. Kim and J. H. Lee, *Biosens. Bioelectron.*, 2011, **26**, 4637–4648.

73 Y. Wang, B. Wang, Q. Zhang, J. Zhao, D. Shi, S. Yunoki, F. Kong and N. Xu, Tunable, *J. Appl. Phys.*, 2012, **111**, 073704.

74 Q. Yue, Z. Shao, S. Chang and J. Li, *Nanoscale Res. Lett.*, 2013, **8**, 1–7.

75 C. Kim, B. Kim, S. M. Lee, C. Jo and Y. H. Lee, *Appl. Phys. Lett.*, 2001, **79**, 1187–1189.

76 Y. Guo, W. Guo and C. Chen, *Appl. Phys. Lett.*, 2008, **92**, 243101.

77 M. Bezi Javan, *J. Mol. Model.*, 2013, **19**, 2273–2283.

78 S. A. Empedocles and M. G. Bawendi, *Science*, 1997, **278**, 2114–2117.

79 Y. Li, Z. R. Li, D. Wu, R. Y. Li, X. Y. Hao and C. C. Sun, *J. Phys. Chem. B*, 2004, **108**, 3145–3148.

80 W. Chen, Z. R. Li, D. Wu, F. L. Gu, X. Y. Hao, B. Q. Wang, R. J. Li and C. C. Sun, *J. Chem. Phys.*, 2004, **121**, 10489–10494.

81 R. L. Zhong, H. L. Xu, Z. R. Li and Z. M. Su, *J. Phys. Chem. Lett.*, 2015, **6**, 612–619.

82 K. Ayub, *J. Mater. Chem. C*, 2016, **4**, 10919–10934.

83 H.-M. He, Y. Li, H. Yang, D. Yu, S. Li, D. Wu, J. Hou, R.-L. Zhong, Z.-J. Zhou, F. L. Gu, J. M. Luis and Z.-R. Li, *J. Phys. Chem. C*, 2017, **121**(1), 958–968.

84 H. Li, H. Xu, X. Shen, K. Han, Z. Bi and R. Xu, *Sci. Rep.*, 1985, **6**, 28067.

85 Y. Bai, Z. J. Zhou, J.-J. Wang, Y. Li, D. Wu, W. Chen, Z.-R. Li and C.-C. Sun, *J. Mol. Model.*, 2013, **19**, 3983–3991.

86 J.-J. Wang, Z.-J. Zhou, H.-M. He, D. Wu, Y. Li, Z.-R. Li and H.-X. Zhang, *J. Phys. Chem. C*, 2016, **120**(25), 13656–13666.

87 S. Nenon and B. Champagne, *J. Phys. Chem. Lett.*, 2014, **5**, 149–153.

88 R. G. Pearson, *J. Org. Chem.*, 1989, **54**, 1423.

89 W. L. Faust, *Science*, 1989, **245**, 37.

90 Z. Zhou and R. G. Parr, *J. Am. Chem. Soc.*, 1990, **112**, 5720.

91 M. Bezi Javan, *Phys. Lett. A*, 2012, **376**, 3241–3247.

92 K. R. Sandip, I. Nazmul and C. G. Dulal, *J. Quantum Inf. Sci.*, 2011, **1**, 87–95.

93 O. Kikuchi, *Quant. Struct.-Act. Relat.*, 1987, **6**, 179.

94 X. Li, S. Deng, H. Fu and T. Li, *Electrochim. Acta*, 2009, **54**, 4089.

95 R. S. Mulliken, *J. Chem. Phys.*, 1934, **2**, 782.

96 A. Soltani, M. Ramezani Taghartapeh, M. Bezi Javan, P. J. Mahon, Z. Azmoodeh, E. Tazikeh Lemeski and I. V. Kityk, *Physica E*, 2018, **97**, 239–249.

97 H. Jacobsen, *Can. J. Chem.*, 2008, **86**, 695–702.

98 A. Komornicki and J. W. McIver, *J. Chem. Phys.*, 1979, **70**, 2014–2016.

99 A. Escobedo-Morales, L. Tepech-Carrillo, A. Bautista-Hernández, J. Humberto Camacho-García, D. Cortes-Arriagada and E. Chigo-Anota, *Sci. Rep.*, 2019, **9**, 16521.

100 E. Chigo Anota, D. Cortes Arriagada, A. Bautista Hernándezc and M. Castro, *Appl. Surf. Sci.*, 2017, **400**, 283–292.

101 H. Shin, J. Guan, M. Z. Zgierski, K. S. Kim, C. T. Kingston and B. Simard, *ACS Nano*, 2015, **9**(12), 12573–12582.

102 T. H. Mahato, G. K. Prasad, B. Singh, K. Batra and K. Ganesan, *Microporous Mesoporous Mater.*, 2010, **132**, 15–21.

103 H. Sohn, S. Letant, M. J. Sailor and W. C. Trogler, *J. Am. Chem. Soc.*, 2000, **122**, 5399.

104 A. J. Mott and P. Rez, *Spectrochim. Acta, Part A*, 2012, **91**, 256–260.

105 Y. Yang, D. Li, C. Li, Y. Liu and K. Jiang, *J. Hazard. Mater.*, 2018, **341**, 93–101.

106 T. H. Mahato, G. K. Prasad, B. Singh, A. R. Srivastava, K. Ganesan, J. Acharya and R. Vijayaraghavan, *J. Hazard. Mater.*, 2009, **166**, 1545–1549.

107 P.-H. Wang, J.-H. Yu, Z.-J. Li, Z.-J. Ding, L. Guo and B. Du, *Sens. Actuators, B*, 2013, **188**, 1306–1311.

108 L. Koponen, L. Tunturivuori, M. J. Puska and R. M. Nieminen, *J. Chem. Phys.*, 2007, **126**, 214306.

109 N. Abdolahi, M. Aghaei, A. Soltani, Z. Azmoodeh, H. Balakheyli and F. Heidari, *Spectrochim. Acta, Part A*, 2018, **204**, 348–353.

110 A. Soltani, M. Ramezani Taghartapeh, V. Erfani-Moghadam, M. Bezi Javan, F. Heidari, M. Aghaei and P. J. Mahon, *Mater. Sci. Eng., C*, 2018, **92**, 216–227.

111 Z. Gao, C. Zhi, Y. Bando, D. Golberg and T. Serizawa, *J. Am. Chem. Soc.*, 2010, **132**, 976.

112 Z. Gao, C. Zhi, Y. Bando, D. Golberg and T. Serizawa, *ACS Appl. Mater. Interfaces*, 2011, **3**, 627–632.